Geophysical Research Letters

RESEARCH LETTER
10.1029/2020GL090668

Seismicity Rate Changes and Geodetic Transients in Central Apennines

Blaž Vičič[1], Abdelkrim Aoudia[1], Alessandra Borghi[1,2], Seyyedmaalek Momeni[1], and Alessandro Vuan[3]

[1]The Abdus Salam International Centre for Theoretical Physics, Trieste, Italy, [2]Istituto Nazionale Geofisica e Vulcanologia, sezione di Bologna, Bologna, Italy, [3]National Institute of Oceanography and Applied Geophysics-OGS, Sgonico, Italy

Key Points:
- Subhorizontal shear zone beneath the shallow normal faults of Central Apennines is segmented into high and low seismicity rate strands
- Rate changes in seismicity are time correlated with a transient deformation observed before the 2016 Central Italy sequence
- *Mw*5+ earthquakes on the Campotosto fault highlight a connection between high-rate shear zone segments and locked fault patches

Supporting Information:
- Supporting Information S1

Correspondence to:
B. Vičič,
bvicic@ictp.it

Citation:
Vičič, B., Aoudia, A., Borghi, A., Momeni, S., & Vuan, A. (2020). Seismicity rate changes and geodetic transients in Central Apennines. *Geophysical Research Letters*, *47*, e2020GL090668. https://doi.org/10.1029/2020GL090668

Received 3 SEP 2020
Accepted 22 OCT 2020
Accepted article online 29 OCT 2020

Abstract Using template matching and GPS data, we investigate the evolution of seismicity and observable deformation in Central Apennines. Seismicity appears more persistent at the base of the seismogenic layer than in the shallower crust. Diffuse activity is reported on segments at depth, alternating along strike with apparent quiescence on segments that experienced one or more *Mw*6+ earthquakes in 1997, 2009, and 2016. Central Apennines are likely underlain by a sizeable shear zone with areas of diffuse seismicity bounding shallow normal faults where *Mw*6+ earthquakes occurred. The deformation observed at the surface seems to follow the seismicity variations at the base of seismogenic layer along the Apenninic chain. Principal and independent component analyses of GPS data exhibit a transient when the 2016 foreshock sequence starts. This transient propagated northward from the Campotosto fault up to the Alto Tiberina fault system and has likely loaded the *Mw*6+ 2016 earthquake sequence.

Plain Language Summary We use a nonstandard method for the detection of microseismicity at depth augmenting the available catalog. The enhanced seismicity distribution is coupled with the observable deformation on a geodetic network of continuous GPS to infer a better comprehension of the earthquake behavior. The earthquake patterns in Central Apennines reveal a segmentation at depth along an almost flat base of seismogenic layer with alternating low and high seismicity rate segments. The deformation recorded at the surface seems to follow the seismicity variations at the base of seismogenic layer along the Apenninic chain also determining a possible seismic-aseismic mode. We suggest that aseismic deformation has a fundamental role in the tectonic loading and that seismicity, even if heterogeneously distributed, could represent a tracer of it. This conclusion is also supported by the evidence of a transient propagating from south to north during the 2016 Central Italy sequence.

1. Introduction

Historical and recent destructive earthquakes in the Central Apennines, Italy (Amato et al., 1998; Chiaraluce et al., 2017; Rovida et al., 2011; Valoroso et al., 2013) occur mostly along the NW-SE trending system of normal faults, where 2 to 3 mm/year of extension perpendicular to the Apennines is accommodated (D'Agostino et al., 2011). The fault system is located above a delaminating Adria lithosphere (Aoudia et al., 2007; Chimera et al., 2003).

Central Apennines were recently struck by three destructive earthquake sequences, namely, Umbria-Marche 1997, L'Aquila 2009, and Amatrice-Visso-Norcia 2016–2017. A number of foreshocks and aftershocks were relocated using both continuous and temporary networks (Amato et al., 1998; Chiaraluce et al., 2011; Improta et al., 2019; Valoroso et al., 2013; Vuan et al., 2017) to depict the geometry of the system. The relocated catalogs of L'Aquila and Amatrice-Visso-Norcia sequences show a subhorizontal, east dipping shear zone (SZ) at the base of the seismogenic volume, between 8 and 12 km. The subhorizontal geometry of SZ is confirmed by focal solutions of foreshocks and aftershocks at the base of Campotosto and Monte Vettore faults (Chiaraluce et al., 2017; Improta et al., 2019; Valoroso et al., 2013). Seismic profiles and geologic cross sections show a horizontal SZ between 8 and 11 km as a transition from sedimentary into basement units (e.g., Porreca et al., 2018). This transition corresponds to the observed velocity changes underneath L'Aquila and Amatrice-Visso-Norcia sequences inferred by earthquake traveltime tomography (Buttinelli et al., 2018; Chiarabba et al., 2018).

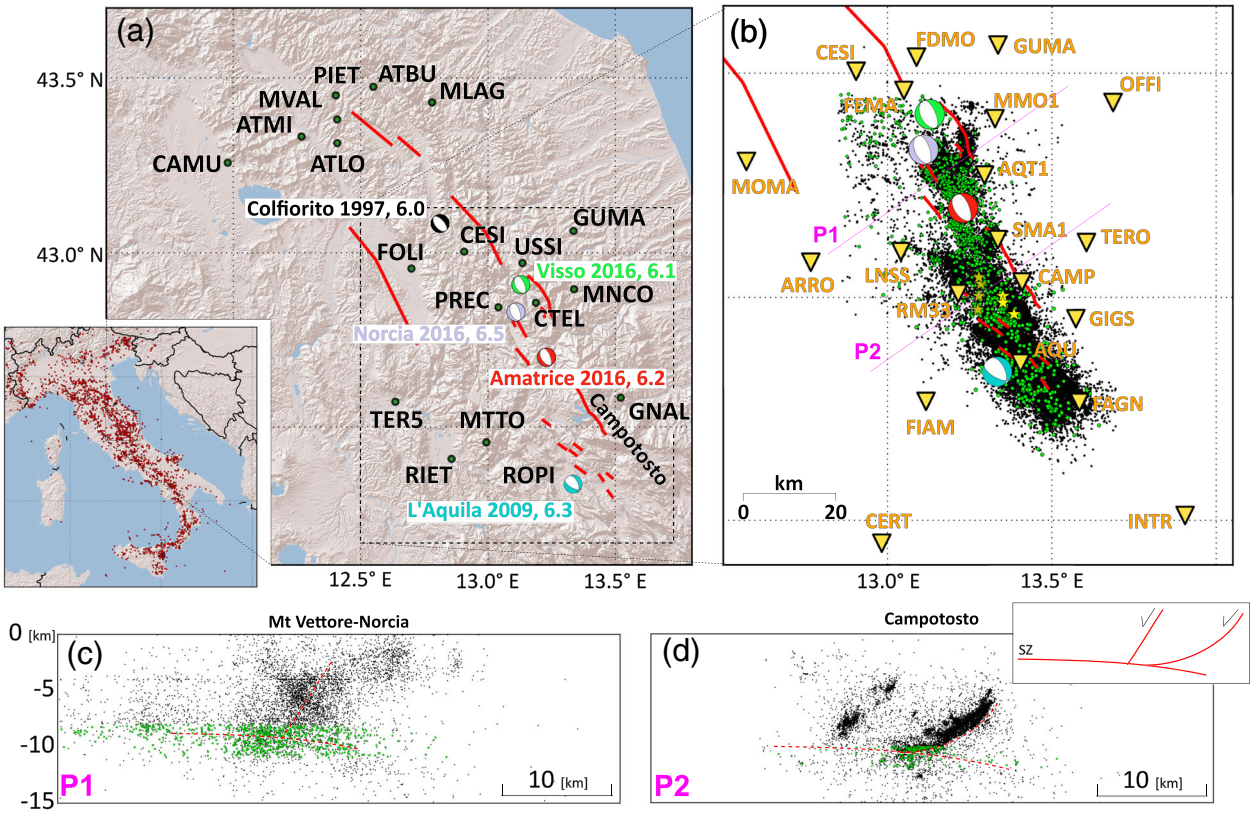

Figure 1. Studied area of Central Italy. (a) Map of destructive earthquakes since 1997 in the studied area. Beach ball colors refer to the same events in Figures 1a and 1b. Red lines represent causative faults responsible for the mainshocks. In green we plot the continuous GPS stations. (b) Triangles represent seismic stations used in this study. Black dots are earthquakes of 2009 L'Aquila and 2016 Amatrice-Visso-Norcia sequences. With green we show selected template earthquakes. (c and d) Cross sections over Amatrice-Visso-Norcia and L'Aquila epicentral areas. In (d) we show an idealized profile over the area with normal faults, mature listric faults, and shear zone.

Before the L'Aquila 2009 mainshock, a foreshock sequence started in the area adjacent to the nucleation point of the *Mw*6.3 mainshock (Valoroso et al., 2013). Sugan et al. (2014) identified three phases of foreshock migration toward the nucleation point of the 6 April 2009 mainshock, with one in mid-February interpreted as a slow-slip transient. The same transient was identified using GPS data by Borghi et al. (2016), who attributed it to a *M*6.1 slow-slip event. It was suggested that the transient took place over a subhorizontal SZ at the base of Paganica and Campotosto faults involving the lateral extent of the aftershock sequence. Before the Amatrice 24 August 2016 earthquake, Vuan et al. (2017) proposed that slip along the SZ increased the stress around the source area of the mainshock, contributing to the unlocking of the overlying normal faults.

Among the mentioned faults, the geometry and seismic potential of the Campotosto fault (Figures 1a and 1d) (hereafter Cf) for producing large earthquakes has been debatable, especially after the 2009 and 2016–2017 *Mw*5+ events (i.e., Cheloni et al., 2014, 2019; Chiaraluce et al., 2011; Falcucci et al., 2018; Gualandi et al., 2014; Valoroso et al., 2013).

Cf is situated in the western flank of the Laga Mountains, with a northwest strike, and dips toward the southwest with a listric geometry, as suggested from seismic data (Chiaraluce et al., 2011). Morphotectonic evidence confirms that Cf has different kinematics than its neighboring Paganica and Mount Vettore-Norcia faults toward the southeast and northwest, respectively (Falcucci et al., 2018). Cf is bounded at a depth of 10 km by SZ (Valoroso et al., 2013) and could be capable of producing an *M*6.4–6.6 earthquake (Falcucci et al., 2018). Two historical earthquakes on Cf were reported (Galadini & Galli, 2003) over the past ~8 ka, with ~1 m of minimum vertical slip.

We investigate both seismicity and deformation observed by the geodetic network of the Central Apennines. We exploit waveform similarity over 11 years from 2008 until the beginning of 2019 to define the spatial and

temporal evolution of detected earthquakes within the SZ and its relation to the reactivated normal faults. To understand the geometry of Cf, we invert the extended source ruptures of eight ($4.4 \leq M \leq 5.4$) earthquakes of the 2009 and 2017 sequences (Figure 1b). We perform a principal component analysis and variational Bayesian independent component analysis of all available continuous GPS (cGPS) stations in the broader region of Central Apennines between 1 January 2015 and 24 August 2016 to detect possible geodetic transients and investigate their significance together with seismicity variations. We study the seismicity pattern of the SZ in the broader area of Central Apennines and compare it with our results.

2. Methods

2.1. Template Matching

We analyze the period from 2008 to the beginning of 2019 using only well-relocated foreshocks and aftershocks of 2009 (Valoroso et al., 2013) and 2016 (Vuan et al., 2017) mainshocks (Figure 1b). These selected events nucleated beneath the computed slip distribution of the mainshocks (Walters et al., 2018) within the SZ at depths between 10–12 km and 8–11 km for 2009 and 2016, respectively. The merged earthquake catalog (supporting information Figures S2 and S3) was used in template matching (Gibbons & Ringdal, 2006; Ross et al., 2019; Shelly et al., 2007) to detect collocated earthquakes and transients (Vičič et al., 2019) within the SZ. Daylong waveform data of selected stations (Figure 1b) are downsampled to 20 Hz and filtered between 2 and 8 Hz. For each event, we compute the theoretical *S* wave arrival time (Krischer et al., 2015) using a suitable velocity model (Herrmann et al., 2011) and trim the three-component data in 5 s waveforms centered on this arrival. We extract the templates for the four closest stations. The signal-to-noise ratio of templates is evaluated by using simple kurtosis-based test (Baillard et al., 2014). Templates that do not satisfy the kurtosis test, or are visually bad, are removed. Template matching detection algorithm as described in Vuan et al. (2018) is applied. For positive detection we set a threshold of 12 times median absolute deviation of the daily stacked cross-correlation function. We only select detected events with interevent times >3 s to not count the same events as multiple due to the detections from different templates. Selected detection inside this time window is the one with highest threshold value. The magnitude of the detection is calculated as the median value of the maximum amplitude ratio for all channels between the template and detected event where a tenfold increase in amplitude corresponds to a unit increase in magnitude (Peng & Zhao, 2009).

2.2. Extended Source Inversion

We invert near-field three-component strong motion records of eight earthquakes ($4.4 \leq M \leq 5.4$) that occurred on the Cf during 2009 and 2017 sequences to study the kinematics of the ruptured area and constrain the geometry of Cf and discuss its seismogenic potential. The elliptical subfault approximation method (Di Carli et al., 2010; Momeni et al., 2019; Ruiz & Madariaga, 2013; Twardzik et al., 2012) is used to retrieve the robust features of the ruptures. For each rupture we look for the best waveform fit to the observations (Figures Sa1–Sa7 in Appendix A) and infer the geometry of the Cf along strike and dip. The details of our inversions are presented in Appendixes A and B.

2.3. GPS

We perform a detailed analysis of the available cGPS stations along the Central Apennines from the Alto Tiberina fault system (ATF) to the north and area of L'Aquila 2009 earthquake to the south (Figure 1a). The 2015–2017 time series of the selected stations are analyzed following the procedure described in Barzaghi and Borghi (2018) that includes the estimate of discontinuities due to station equipment changes, seismic events, periodic signals, and a linear velocity term. The temporal correlations among data have been considered as well. The data were spatially filtered to remove correlated noise using the principal component analysis (PCA), as suggested by Dong et al. (2006) in order to search for transients (Borghi et al., 2016; Gualandi et al., 2016). The residual coordinate time series were analyzed using different blind source separation methods (BSS), like Fast Independent Component Analysis (fastICA) and variational Bayesian independent component analysis (vbICA) (Choudrey & Roberts, 2003), as well as PCA. The methodology is described in the supporting information (Appendix C).

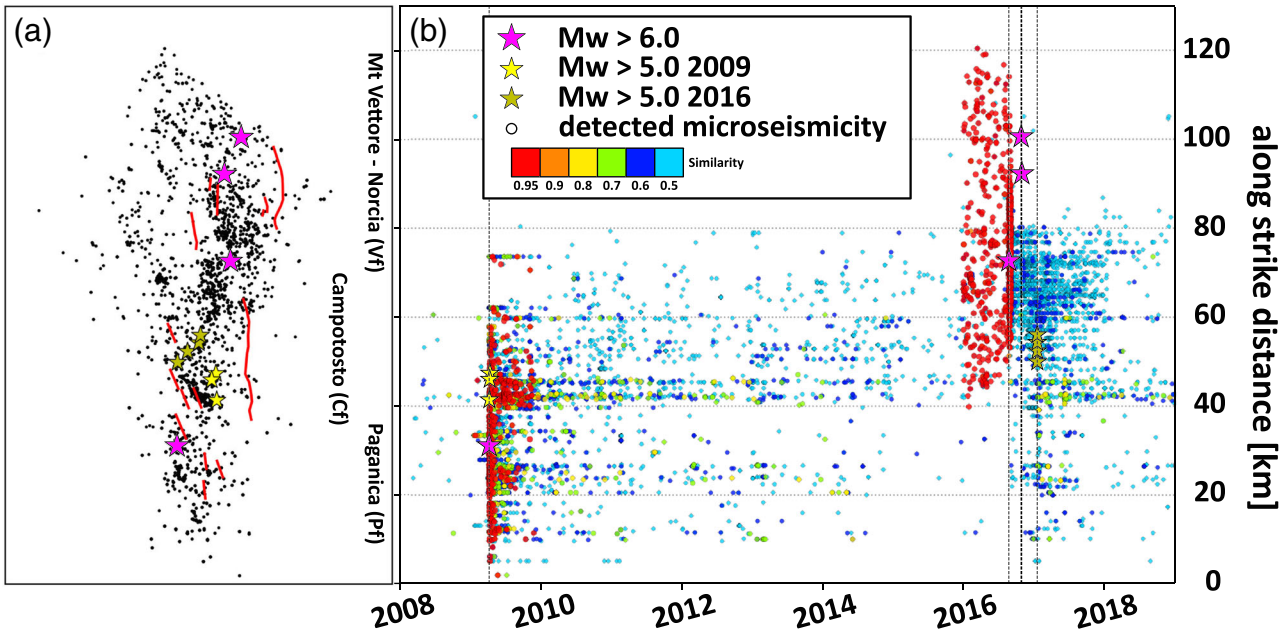

Figure 2. (a) Locations of selected SZ template earthquakes along strike of the Central Italy faults activated in 2009 and 2016 sequences. (b) Newly detected earthquakes from 2008 until the end of 2018. Color represents the cross-correlation value of the detection. The 2009 sequence undergoes a decay of seismicity along the SZ of Paganica fault, while the SZ underneath Campotosto fault shows more constant diffuse earthquake activity. At the beginning of 2016, foreshock activity of 2016 sequence starts along the SZ underneath Campotosto fault and SZ beneath Mount Vettore fault system.

3. The 2009–2016 Sequences

3.1. Detected Earthquakes

To evaluate spatial and temporal evolution of earthquake activity within the SZ, we used 1,855 templates well distributed along strike and throughout the SZ beneath the causative faults of 2009 (10–12 km depth) and 2016–2017 (8–11 km depth) sequences (Figure 2a). We analyze the continuous waveform series from 2008 to 2019 and detect 38,229 new events in the SZ, ranging between M −1.5 and M4.7 (Figures S2 and S8).

Figure 2b shows the along-strike space-time distribution of the newly detected earthquakes (cross-correlation values above 0.5). For the analysis, the whole SZ volume is divided into three subvolumes following the main normal faults: the Paganica fault (Pf) Cf, and the Mount Vettore-Norcia fault (Vf) (e.g., Basili et al., 2018). Beneath Pf, we detect the foreshocks (Figure S9) to the L'Aquila mainshock as reported in Sugan et al. (2014). After the L'Aquila mainshock, the detections exhibit a decay of aftershocks as in Chiaraluce et al. (2011). On the contrary, diffuse earthquakes with slow decay rate are reported within the SZ under the Cf (Figures 1a and 1d). We separate the templates of 2016 sequence into foreshocks and early aftershocks (Figures S4a and S4b) inherent to the 24 August earthquake covering an 80 km along-strike distance that includes Cf and Vf. For Cf, the detections reveal a high rate of activity, independent of the templates we use, over the 11 year time span. Underneath Vf (Figures 1a and 1c), very few new earthquakes are detected, except in its southeasternmost part, adjacent to Cf.

The cumulative number of events over time and their yearly contributions are reported in Figures S5 and S6. We observe that soon after the 2009 mainshock and its aftershock sequence (September 2009), the cumulative number of earthquakes within the SZ beneath Cf overtakes the cumulative number under the Pf. This is true throughout the years 2010–2015, with few exceptions when a small sequence starts along Pf (February 2011, February 2012, and March 2013). The cumulative number of earthquakes beneath Cf is steady over the years and characterizes the background seismicity with small increments over temporal fluctuations (van den Ende & Ampuero, 2020).

At the end of 2015, the number of detections increased beneath Vf, starting the foreshock sequence of the 24 August 2016 Mw6 earthquake. Beneath Cf an intensive swarm took place during February 2016, located adjacent to the future termination of the mainshock slip distribution (Chiaraluce et al., 2017). After the

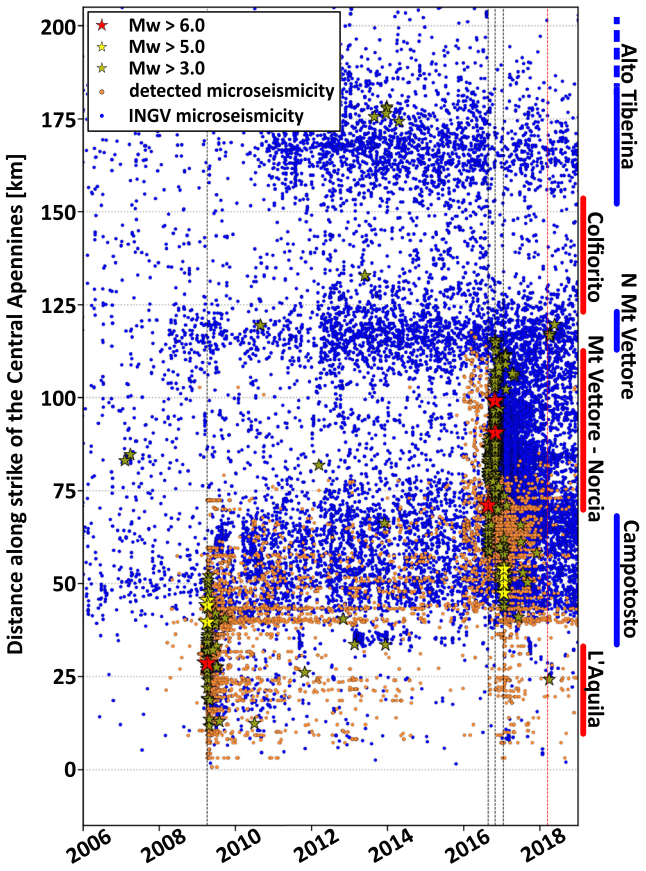

Figure 3. Seismicity along the strike of Central Apennines. Orange dots represent the new earthquakes obtained in this study, while blue dots represent earthquakes deeper than 12 km from Istituto Nazionale di Geofisica e Vulcanologia (INGV) earthquake catalog. We observe good spatial correlation between our enhanced catalog in the 2009 and 2016 epicentral areas and INGV catalog. Additionally, similar behavior is observed along strike of the Central Apennines. Along the segmented SZ we observe segments of high-rate seismicity (Campotosto, north Mount Vettore, Alto Tiberina = blue vertical lines on the right) and segments with low rate of seismicity (L'Aquila, Mount Vettore-Norcia, Colfiorito = red vertical lines on the right). Later correspond to the SZ beneath the faults that ruptured with recent *Mw*6+ events.

swarm, the SZ beneath Vf becomes the most active segment. The diffuse aftershocks that followed the 24 August mainshock are beneath Cf and Vf, where most of the events took place. After the largest mainshock of 30 October, the activity beneath Cf increases, and by the end of 2016 activity beneath Pf starts to increase. Increased earthquake production in late December 2016 beneath Cf signals the foreshock sequence of the 18 January 2017 *Mw*5+ Campotosto earthquakes.

We observe (supporting information Figure S7) a slow (6 km/year) northwestward migration of seismicity from the SZ beneath Pf toward the nucleation area of the 24 August 2016 mainshock. This is followed by a southeastward migration (0.2 km/day) from the 24 August 2016 nucleation area toward the hypocenters of Campotosto 2017 earthquakes similar to the observed migration of seismicity independent of the depth distribution reported by Sebastiani et al. (2019).

3.2. Rupture History for the Cf Moderate Earthquakes

The reported difference between coseismic and aseismic moment released along the Cf during the 2009 and 2017 sequences (e.g., Cheloni et al., 2014, 2019) led to the detailed investigation of the coseismic slip and source geometry of *Mw*5+ earthquakes on Cf.

Seven of the events (except the subhorizontal 22 June 2009 M_L4.4 event along SZ) occurred on planes with strikes from 142° to 190°, on average 157°, dipping to the southwest (supporting information Appendix A Table A1). Our results confirm the listric geometry of Cf with dip changing over depth from 50° to 30° (Figure S1).

All slip models cover an area of ~18 km per 12 km on the Cf. The patches of maximum slip do not overlap, and the ruptures evolved mostly updip. Similar to the migration observed along the SZ after 2009 and 2016 sequence, also the 2009 and 2017 Campotosto *Mw*5+ events follow a similar pattern and migrate from southeast toward northwest after 2009 and vice versa after 2016. Unilateral ruptures are confirmed by directivity in the accelerograms.

Source parameters of the 2009 sequence show an average strike of 152° and dip of 48° for the southeastern part of the Cf. Scalar seismic moment of $1.73 * 10^{17}$ Nm for the three large aftershocks and the SZ event of 2009 are close to the value of $1.8 * 10^{17}$ Nm, obtained using point source inversion method by Scognamiglio et al. (2010). Using synthetic aperture radar (SAR) and GPS data, Cheloni et al. (2014) obtained a cumulative scalar seismic moment of $3.17 * 10^{17}$ Nm for coseismic and postseismic periods in 2009, and Gualandi et al. (2014) calculated an afterslip of a $2.9 * 10^{17}$ Nm released for 301 days after the 2009 mainshock. This suggests that most of the deformation was aseismic with half as postseismic considering negligible sum of the seismic moments released by the rest of the aftershocks (Falcucci et al., 2018).

Average strike for the 2017 events (northwestern part of the Cf) is 161°, while average dip is 35°, 13° less than Falcucci et al. (2018) from inversion of surface deformation measured from cGPS and DInSAR. In their study, the rake angle would play an important role in obtaining the dip angle, while in our inversions the rake was a well-retrieved parameter. The slip models distribute from depths of 2.5 to 10 km with a maximum slip of 0.49 m close to Falcucci et al. (2018). We obtain $7.98 * 10^{17}$ Nm of scalar seismic energy release during 2017 sequence close to the obtained value by Falcucci et al. (2018). Considering $0.4 * 10^{17}$ Nm of scalar seismic moment released by $3.5 < M < 4.9$ aftershocks and the cumulative geodetic moment of $9.29 * 10^{17}$ Nm (Cheloni et al., 2019), we reach the same 35% contribution of aseismic strain release suggested by Cheloni et al. (2019).

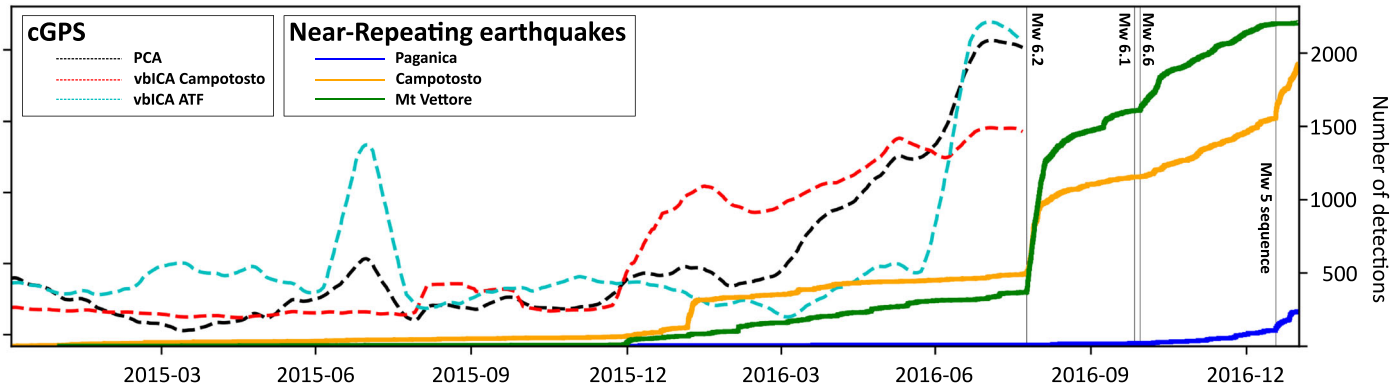

Figure 4. Cumulative number of newly detected earthquakes between 2015 and 2017 and a geodetic transient. Different colors represent different segments of SZ under the shallow normal faults. Dashed black line represents second principal component over all the GPS stations used, while red and magenta represent independent components of spatially grouped cGPS stations, around Campotosto and ATF, respectively. We observe that deformation is migrating from the south of the system toward north.

The computed slip history of the *Mw*5+ events indicate that Cf is partially reactivated along its deeper extent and a rupture up to the surface would require a larger-magnitude earthquake as reported by paleoseismologic observations (e.g., Galadini & Galli, 2003).

4. Central Apennines

4.1. Seismicity

We compare our newly constrained catalog with the Italian Seismic Bulletin (Figure 3). We remove earthquakes shallower than 12 km (removing fixed depth and shallow events) along the Central Apennines. We observe alternating high and low seismicity rate strands along the strike, showing similarities to our own findings in the SZ beneath Pf, Cf, and Vf. The areas of last moderate earthquakes in 1997, 2009, and 2016 correspond to strands where seismicity is less diffuse. The high seismicity rate segments are located in between, namely, Campotosto segment, North Mount Vettore segment (NVf), and Alto Tiberina segment (Anderlini et al., 2016).

4.2. GPS Analysis for Transient Detection

The central part of the network (Figure 1a), where the 2016 *M*6+ events nucleated, represents an empty zone since no stations were installed in that period or we do not have access to the data.

As the analyzed period is quite long (from 2012 to the middle of 2018) and is characterized by the important 2016 seismic sequence, we conducted our analysis dividing the time series into four different temporal windows. In this section we focus on the 2015–2016 and 2017–2018 temporal windows, but all the results of the other periods are reported in Appendix C.

Although the vbICA method has resulted to be efficient in finding the signal along the ATF (Gualandi et al., 2017, and Appendix C), we also applied the PCA method in the analysis of the period characterized by the 2016 seismic sequence, to find the average behavior of the stations and avoid local effects, which allow the vbICA to better identify the signals. We show the results (Figure 4) in terms of the second principal component (PC2) of the east component. We observe an increase of values starting at the beginning of 2016 with both northern (ATF) and southern (Campotosto) GPS station clusters contributing to the PC2. We repeat the analysis splitting the stations in the ATF and in the Campotosto part. Analyzing the two clusters separately allowed us to point out a similar behavior of the ATF and Campotosto stations but shifted in time: the Campotosto stations present this discontinuity in the first vbICA component on 7 January 2016, with a probability around 94% as detected by the Bayesian test inference (Appendix C), whereas the ATF stations present an analogous behavior 7 months later on 7 July with a probability of 98% (Figure 4).

The analysis of the last period, from the end of 2017 to April 2018, involves the cGPS stations set up after the *Mw*6.5 earthquake on 30 October 2016. The time series show (Appendix C Figure Sc6) the nonlinear effect of the postseismic deformation. Accordingly, we preferred not to fit the data using any functional models but

applied the PCA to describe the deformation. In Appendix C Figures Sc7 and Sc8 the north and east first principal components are reported. All the stations are affected by a common signal represented by the linear tectonic rate and the postseismic deformations; however, a discontinuity is present at the beginning of 2018. Soon after the discontinuity, the northern extension of the area affected by three *Mw*6+ earthquakes is hit by a series of *Mw*3.5+ earthquakes with the strongest *Mw*4.5 on 10 April 2018.

5. Conclusions

Analyzing 11 years of continuous waveforms recorded at multiple seismic stations in Central Italy allowed us to detect more than 38,000 earthquakes within the SZ. The detected events and their locations give us insight on the space-time behavior of the SZ underneath Pf, Cf, and Monte Vettore fault (Vf) before, after, and in between the recent Central Italy earthquake sequences. Pf and Vf are related to the 2009 *Mw*6.1 L'Aquila earthquake and the 2016 Amatrice-Visso-Norcia *Mw*6+ earthquakes, respectively, which ruptured shallow, SW dipping normal faults. Cf, located in between Pf and Vf, is affected in the aftermath of both 2009 and 2016 sequences with earthquakes of *Mw*5+. We observe different spatial and temporal patterns of earthquakes within the SZ underneath Pf, Cf, and Vf.

The seismicity rate within the SZ appears to be segmented from south to north along the strike of the fault system (Figure 3). SZ beneath Pf is experiencing an expected decay in its activity after the 2009 earthquake reaching a lower rate with very few events after 2014, while the adjacent SZ beneath Cf exhibits a far higher rate in its activity. The SZ beneath Vf shows a very low rate between 2009 up to the end of 2015 when it starts exhibiting a large foreshock sequence, also affecting SZ beneath Cf as well as the above normal faults, prior to the 2016 *Mw*6+ earthquakes.

Our study suggests that Central Apennines are underlain by a sizeable subhorizontal SZ that is segmented in its frictional and/or mechanical properties accommodating therefore low and high rates of seismicity at the base of the seismogenic layer. The low-rate seismicity segments are beneath high-angle normal faults responsible for the 1997, 2009, and 2016 earthquake sequences. The high-rate seismicity segments are beneath listric faults (e.g., Campotosto) and low-angle normal faults like Alto Tiberina (e.g., Chiaraluce et al., 2014).

Analyzing 19 cGPS stations show that the start of the 2016 foreshock sequence coincides with a clear geodetic transient that first affected Cf-Pf and later expanded northward affecting ATF. The foreshocks likely correspond to creeping patches accommodating aseismic slow slip in the preseismic period (e.g., Meng et al., 2015) combined with a gradual unlocking within the plate boundary (e.g., Schurr et al., 2014). The space-time correlations between the seismicity and the geodetic transient and their northward along-strike migrations are thus most likely due to an expanding/propagating slow slip along strike. These results together with the space distribution of the mainshocks show that, most likely, the northward expanding transient was accommodated differently by the reactivated fault system where less-coupled segments alternate with locked segments. Similar behavior is described in subduction zones (e.g., Radiguet et al., 2016; Rolandone et al., 2018). Furthermore, we argue that the geometry and the frictional properties of the segmented system affects the degree of interseismic coupling. This likely leads to differences in recurrence intervals and maximum magnitude between mature listric faults and younger high-angle normal faults as exhibited by the historical seismicity and paleoseismology across Central Apennines (e.g., Cinti et al., 2018; Falcucci et al., 2018; Galadini & Galli, 2003; Galli et al., 2019; Guidoboni et al., 2018).

Acknowledgments
The authors would like to thank Generali group and Generali Italia for the financial support. We would like to thank the Editor and the three reviewers for their useful comments that improved our original manuscript. PyMPA software (Vuan et al., 2018) development is partly supported by the project "Real-time earthquake rIsk reduction for a reSilient Europe" (RISE), financed by the Horizon 2020 program of the European Commission.

Data Availability Statement

The data are available via the European Integrated Data Archive managed by Istituto Nazionale di Geofisica e Vulcanologia (INGV) (http://www.orfeus-eu.org/webdc3/) and Nevada Geodetic Laboratory (http://geodesy.unr.edu/index.php).

References

Amato, A., Azzara, R., Chiarabba, C., Cimini, G. B., Cocco, M., di Bona, M., et al. (1998). The 1997 Umbria-Marche, Italy, earthquake sequence: A first look at the main shocks and aftershocks. *Geophysical Research Letters*, *25*(15), 2861–2864. https://doi.org/10.1029/98GL51842

Anderlini, L., Serpelloni, E., & Belardinelli, M. E. (2016). Creep and locking of a low-angle normal fault: Insights from the Altotiberina fault in the northern Apennines (Italy). *Geophysical Research Letters*, *43*, 4321–4329. https://doi.org/10.1002/2016GL068604

Aoudia, A., Ismail-Zadeh, A. T., & Romanelli, F. (2007). Buoyancy-driven deformation and contemporary tectonic stress in the lithosphere beneath Central Italy. *Terra Nova*, *19*(6), 490–495. https://doi.org/10.1111/j.1365-3121.2007.00776.x

Baillard, C., Crawford, W., Ballu, V., Hilbert, C., & Mangeney, A. (2014). Kurtosis-based *P* and *S* phase picker designed for local and regional seismic networks. *Bulletin of the Seismological Society of America*, *104*(1). https://doi.org/10.1785/0120120347

Barzaghi, R., & Borghi, A. (2018). Theory of second order stationary random processes applied to GPS coordinate time-series. *GPS Solutions*, *22*(3), 1–12. https://doi.org/10.1007/s10291-018-0748-4

Basili, R., Burrato, P., Fracassi, U., Kastelic, V., Maesano, F., Tarabusi, G., et al. (2018). Database of Individual Seismogenic Sources (DISS), Version 3.2. 1: A compilation of potential sources for earthquakes larger than *M* 5.5 in Italy and surrounding areas. https://doi.org/10.6092/INGV.IT-DISS3.2.1

Borghi, A., Aoudia, A., Javed, F., & Barzaghi, R. (2016). Precursory slow-slip loaded the 2009 L'Aquila earthquake sequence. *Geophysical Journal International*, *205*, 776–784. https://doi.org/10.1093/gji/ggw046

Buttinelli, M., Pezzo, G., Valoroso, L., De Gori, P., & Chiarabba, C. (2018). Tectonics inversions, fault segmentation, and triggering mechanisms in the Central Apennines normal fault system: Insights from high-resolution velocity models. *Tectonics*, *37*, 4135–4149. https://doi.org/10.1029/2018TC005053

Cheloni, D., D'Agostino, N., Scognamiglio, L., Tinti, E., Bignami, C., Avallone, A., et al. (2019). Heterogeneous behavior of the Campotosto normal fault (Central Italy) imaged by InSAR GPS and strong-motion data: Insights from the 18 January 2017 events. *Remote Sensing*, *11*(12), 1482. https://doi.org/10.3390/rs11121482

Cheloni, D., Giuliani, R., D'Anastasio, E., Atzori, S., Walters, R. J., Bonci, L., et al. (2014). Coseismic and post-seismic slip of the 2009 L'Aquila (Central Italy) *Mw*6.3 earthquake and implications for seismic potential along the Campotosto fault from joint inversion of high-precision levelling, InSAR and GPS data. *Tectonophysics*, *622*, 168–185. https://doi.org/10.1016/j.tecto.2014.03.009

Chiarabba, C., De Gori, P., Cattaneo, M., Spallarossa, D., & Segou, M. (2018). Faults geometry and the role of fluids in the 2016–2017 Central Italy seismic sequence. *Geophysical Research Letters*, *45*, 6963–6971. https://doi.org/10.1029/2018GL077485

Chiaraluce, L., Amato, A., Carannante, S., Castelli, V., Cattaneo, M., Cocco, M., et al. (2014). The Alto Tiberina near fault observatory (northern Apennines, Italy). *Annals of Geophysics*, *57*(3). https://doi.org/10.4401/ag-6426

Chiaraluce, L., Di Stefano, R., Tinti, E., Scognamiglio, L., Michele, M., Casarotti, E., et al. (2017). The 2016 Central Italy seismic sequence: A first look at the mainshocks, aftershocks, and source models. *Seismological Research Letters*, *88*(3), 757–771. https://doi.org/10.1785/0220160221

Chiaraluce, L., Valoroso, L., Piccinini, D., Di Stefano, R., & De Gori, P. (2011). The anatomy of the 2009 L'Aquila normal fault system (Central Italy) imaged by high resolution foreshock and aftershock locations. *Journal of Geophysical Research*, *116*, B12311. https://doi.org/10.1029/2011JB008352

Chimera, G., Aoudia, A., Saraò, A., & Panza, G. F. (2003). Active tectonics in Central Italy: Constraints from surface wave tomography and source moment tensor inversion. *Physics of the Earth and Planetary Interiors*, *138*(3–4), 241–262. https://doi.org/10.1016/S0031-9201(03)00152-3

Choudrey, R. A., & Roberts, S. J. (2003). Variational mixture of Bayesian independent component analyzers. *Neural Computation*, *15*(1), 213–252. https://doi.org/10.1162/089976603321043766

Cinti, F. R., Civico, R., Blumetti, A. M., Chiarini, E., la Posta, E., Pantosti, D., et al. (2018). Evidence for surface faulting earthquakes on the Montereale fault system (Abruzzi Apennines, Central Italy). *Tectonics*, *37*, 2758–2776. https://doi.org/10.1029/2017TC004780

D'Agostino, N., Mantenuto, S., D'Anastasio, E., Giuliani, R., Mattone, M., Calcaterra, S., et al. (2011). Evidence for localized active extension in the Central Apennines (Italy) from global positioning system observations. *Geology*, *39*(4), 291–294. https://doi.org/10.1130/G31796.1

Di Carli, S., François-Holden, C., Peyrat, S., & Madariaga, R. (2010). Dynamic inversion of the 2000 Tottori earthquake based on elliptical subfault approximations. *Journal of Geophysical Research*, *115*, B12238. https://doi.org/10.1029/2009JB006358

Dong, D., Fang, P., Bock, Y., Webb, F., Prawirodirdjo, L., Kedar, S., & Jamason, P. (2006). Spatiotemporal filtering using principal component analysis and Karhunen-Loeve expansion approaches for regional GPS network analysis. *Journal of Geophysical Research*, *111*, B03405. https://doi.org/10.1029/2005JB003806

Falcucci, E., Gori, S., Bignami, C., Pietrantonio, G., Melini, D., Moro, M., et al. (2018). The Campotosto seismic gap in between the 2009 and 2016–2017 seismic sequences of Central Italy and the role of inherited lithospheric faults in regional seismotectonic settings. *Tectonics*, *37*, 2425–2445. https://doi.org/10.1029/2017TC004844

Galadini, F., & Galli, P. (2003). Paleoseismology of silent faults in the Central Apennines (Italy): The Mt. Vettore and Laga Mts. Faults. *Annals of Geophysics*. https://doi.org/10.4401/ag-3457

Galli, P., Galderisi, A., Peronace, E., Giaccio, B., Hajdas, I., Messina, P., et al. (2019). The awakening of the dormant Mount Vettore fault (2016 Central Italy earthquake, *Mw*6.6): Paleoseismic clues on its millennial silences. *Tectonics*, *38*, 687–705. https://doi.org/10.1029/2018TC005326

Gibbons, S. J., & Ringdal, F. (2006). The detection of low magnitude seismic events using array-based waveform correlation. *Geophysical Journal International*, *165*(1), 149–166. https://doi.org/10.1111/j.1365-246X.2006.02865.x

Gualandi, A., Nichele, C., Serpelloni, E., Chiaraluce, L., Anderlini, L., Latorre, D., et al. (2017). Aseismic deformation associated with an earthquake swarm in the northern Apennines (Italy). *Geophysical Research Letters*, *44*, 7706–7714. https://doi.org/10.1002/2017GL073687

Gualandi, A., Serpelloni, E., & Belardinelli, M. E. (2014). Space–time evolution of crustal deformation related to the M_w6.3, 2009 L'Aquila earthquake (Central Italy) from principal component analysis inversion of GPS position time-series. *Geophysical Journal International*, *197*(1), 174–191. https://doi.org/10.1093/gji/ggt522

Gualandi, A., Serpelloni, E., & Belardinelli, M. E. (2016). Blind source separation problem in GPS time series. *Journal of Geodesy*, *90*(4), 323–341. https://doi.org/10.1007/s00190-015-0875-4

Guidoboni, E., Ferrari, G., Mariotti, D., Comastri, A., Tarabusi, G., Sgattoni, G., & Valensise, G. (2018). CFTI5Med, Catalogo dei Forti Terremoti in Italia (461 aC-1997) e nell'area Mediterranea (760 aC-1500), https://doi.org/10.6092/ingv.it-cfti5

Herrmann, R. B., Malagnini, L., & Munafò, I. (2011). Regional moment tensors of the 2009 L'Aquila earthquake sequence regional moment tensors of the 2009 L'Aquila earthquake sequence. *Bulletin of the Seismological Society of America*, *101*(3), 975–993. https://doi.org/10.1785/0120100184

Improta, L., Latorre, D., Margheriti, L., Nardi, A., Marchetti, A., Lombardi, A. M., et al. (2019). Multi-segment rupture of the 2016 Amatrice-Visso-Norcia seismic sequence (Central Italy) constrained by the first high-quality catalog of early aftershocks. *Scientific Reports*, *9*(1), 1–13. https://doi.org/10.1038/s41598-019-43393-2

Krischer, L., Megies, T., Barsch, R., Beyreuther, M., Lecocq, T., Caudron, C., & Wassermann, J. (2015). ObsPy: A bridge for seismology into the scientific Python ecosystem. *Computational Science & Discovery*, *8*(1), 014003. https://doi.org/10.1088/1749-4699/8/1/014003

Meng, L., Huang, H., Bürgmann, R., Ampuero, J. P., & Strader, A. (2015). Dual megathrust slip behaviors of the 2014 Iquique earthquake sequence. *Earth and Planetary Science Letters*, *411*, 177–187. https://doi.org/10.1016/j.epsl.2014.11.041

Momeni, S. M., Aoudia, A., Tatar, M., Twardzik, C., & Madariaga, R. (2019). Kinematics of the 2012 Ahar–Varzaghan complex earthquake doublet (M_w6.5 and M_w6.3). *Geophysical Journal International*, *217*(3), 2097–2124. https://doi.org/10.1093/gji/ggz100

Peng, Z., & Zhao, P. (2009). Migration of early aftershocks following the 2004 Parkfield earthquake. *Nature Geoscience*, *2*(12), 877–881. https://doi.org/10.1038/ngeo697

Porreca, M., Minelli, G., Ercoli, M., Brobia, A., Mancinelli, P., Cruciani, F., et al. (2018). Seismic reflection profiles and subsurface geology of the area interested by the 2016–2017 earthquake sequence (Central Italy). *Tectonics*, *37*, 1116–1137. https://doi.org/10.1002/2017TC004915

Radiguet, M., Perfettini, H., Cotte, N., Gualandi, A., Valette, B., Kostoglodov, V., et al. (2016). Triggering of the 2014 M_w7.3 Papanoa earthquake by a slow slip event in Guerrero, Mexico. *Nature Geoscience*, *9*(11), 829–833. https://doi.org/10.1038/ngeo2817

Rolandone, F., Nocquet, J. M., Mothes, P. A., Jarrin, P., Vallée, M., Cubas, N., et al. (2018). Areas prone to slow slip events impede earthquake rupture propagation and promote afterslip. *Science Advances*, *4*(1), eaao6596. https://doi.org/10.1126/sciadv.aao6596

Ross, Z. E., Trugman, D. T., Hauksson, E., & Shearer, P. M. (2019). Searching for hidden earthquakes in Southern California. *Science*, *364*(6442), 767–771. https://doi.org/10.1126/science.aaw6888

Rovida, A., Camassi, R., Gasperini, P., & Stucchi, M. (2011). Catalogo parametrico dei terremoti italiani. https://doi.org/10.13127/CPTI/CPTI15.2

Ruiz, S., & Madariaga, R. (2013). Kinematic and dynamic inversion of the 2008 northern Iwate earthquake. *Bulletin of the Seismological Society of America*, *103*(2A), 694–708. https://doi.org/10.1785/0120120056

Schurr, B., Asch, G., Hainzl, S., Bedford, J., Hoechner, A., Palo, M., et al. (2014). Gradual unlocking of plate boundary controlled initiation of the 2014 Iquique earthquake. *Nature*, *512*(7514), 299–302. https://doi.org/10.1038/nature13681

Scognamiglio, L., Tinti, E., Michelini, A., Dreger, D. S., Cirella, A., Cocco, M., et al. (2010). Fast determination of moment tensors and rupture history: What has been learned from the 6 April 2009 L'Aquila earthquake sequence. *Seismological Research Letters*, *81*(6), 892–906. https://doi.org/10.1785/gssrl.81.6.892

Sebastiani, G., Govoni, A., & Pizzino, L. (2019). Aftershock patterns in recent Central Apennines sequences. *Journal of Geophysical Research: Solid Earth*, *124*, 3881–3897. https://doi.org/10.1029/2018JB017144

Shelly, D. R., Beroza, G. C., & Ide, S. (2007). Non-volcanic tremor and low-frequency earthquake swarms. *Nature*, *446*(7133), 305–307. https://doi.org/10.1038/nature05666

Sugan, M., Kato, A., Miyake, H., Nakagawa, S., & Vuan, A. (2014). The preparatory phase of the 2009 *Mw*6.3 L'Aquila earthquake by improving the detection capability of low-magnitude foreshocks. *Geophysical Research Letters*, *41*, 6137–6144. https://doi.org/10.1002/2014GL061199

Twardzik, C., Madariaga, R., Das, S., & Custódio, S. (2012). Robust features of the source process for the 2004 Parkfield, California, earthquake from strong-motion seismograms. *Geophysical Journal International*, *191*(3), 1245–1254. https://doi.org/10.1111/j.1365-246X.2012.05653.x

Valoroso, L., Chiaraluce, L., Piccinini, D., Di Stefano, R., Schaff, D., & Waldhauser, F. (2013). Radiography of a normal fault system by 64,000 high-precision earthquake locations: The 2009 L'Aquila (Central Italy) case study. *Journal of Geophysical Research: Solid Earth*, *118*, 1156–1176. https://doi.org/10.1002/jgrb.50130

van den Ende, M. P., & Ampuero, J. P. (2020). On the statistical significance of foreshock sequences in Southern California. *Geophysical Research Letters*, *47*, e2019GL086224. https://doi.org/10.1029/2019GL086224

Vičič, B., Aoudia, A., Javed, F., Foroutan, M., & Costa, G. (2019). Geometry and mechanics of the active fault system in western Slovenia. *Geophysical Journal International*, *217*(3), 1755–1766. https://doi.org/10.1093/gji/ggz118

Vuan, A., Sugan, M., Amati, G., & Kato, A. (2018). Improving the detection of low-magnitude seismicity preceding the M_w6.3 L'Aquila earthquake: Development of a scalable code based on the cross correlation of template earthquakes. *Bulletin of the Seismological Society of America*, *108*(1), 471–480. https://doi.org/10.1785/0120170106

Vuan, A., Sugan, M., Chiaraluce, L., & Di Stefano, R. (2017). Loading rate variations along a midcrustal shear zone preceding the *Mw*6.0 earthquake of 24 August 2016 in Central Italy. *Geophysical Research Letters*, *44*, 12,170–12,180. https://doi.org/10.1002/2017GL076223

Walters, R. J., Gregory, L. C., Wedmore, L. N. J., Craig, T. J., McCaffrey, K., Wilkinson, M., et al. (2018). Dual control of fault intersections on stop-start rupture in the 2016 Central Italy seismic sequence. *Earth and Planetary Science Letters*, *500*, 1–14. https://doi.org/10.1016/j.epsl.2018.07.043

References From the Supporting Information

Blewitt, G., Hammond, W. C., & Kreemer, C. (2018). Harnessing the GPS data explosion for interdisciplinary science. *Eos*, *99*, 1–2. https://doi.org/10.1029/2018EO104623

Borghi, A., Aoudia, A., Riva, R., & Barzaghi, R. (2009). GPS monitoring and earthquake prediction: A success story towards a useful integration. *Tectonophysics*, *465*, 177–189, ISSN 0040-1951. https://doi.org/10.1016/j.tecto.2008.11.022

Borghi, A., Cannizzaro, L., & Vitti, A. (2012). Advanced techniques for discontinuity detection in GNSS coordinate time-series. An Italian case study. In *Geodesy for planet Earth* (pp. 627–634). Berlin, Heidelberg: Springer. https://doi.org/10.1007/978-3-642-20338-1_77

Choudrey, R.A. (2002). Variational methods for Bayesian independent component analysis. Pattern analysis and machine learning—Robotics research group, University of Oxford.

Cotton, F., & Coutant, O. (1997). Dynamic stress variations due to shear faults in a plane-layered medium. *Geophysical Journal International*, *128*(3), 676–688. https://doi.org/10.1111/j.1365-246X.1997.tb05328.x

Hyvärinen, A., & Oja, E. (2000). Independent component analysis: Algorithms and applications. *Neural Networks*, *13*(4–5), 411–430. https://doi.org/10.1016/S0893-6080(00)00026-5

Sambridge, M. (1999a). Geophysical inversion with a neighbourhood algorithm—I. Searching a parameter space. *Geophysical Journal International*, *138*(2), 479–494. https://doi.org/10.1046/j.1365-246X.1999.00876.x

Sambridge, M. (1999b). Geophysical inversion with a neighbourhood algorithm—II. Appraising the ensemble. *Geophysical Journal International*, *138*(3), 727–746. https://doi.org/10.1046/j.1365-246x.1999.00900.x

Schmedes, J., Archuleta, R. J., & Lavallée, D. (2010). Correlation of earthquake source parameters inferred from dynamic rupture simulations. *Journal of Geophysical Research*, *115*, B03304. https://doi.org/10.1029/2009JB006689

Silverii, F., D'Agostino, N., Borsa, A. A., Calcaterra, S., Gambino, P., Giuliani, R., & Mattone, M. (2019). Transient crustal deformation from karst aquifers hydrology in the Apennines (Italy). *Earth and Planetary Science Letters*, *506*, 23–37. https://doi.org/10.1016/j.epsl.2018.10.019

Spudich, P., & Miller, D. P. (1990). Seismic site effects and the spatial interpolation of earthquake seismograms: Results using aftershocks of the 1986 North Palm Springs, California, earthquake. *Bulletin of the Seismological Society of America*, *80*(6A), 1504–1532.

Wdowinski, S., Bock, Y., Zhang, J., Fang, P., & Genrich, J. (1997). Southern California permanent GPS geodetic array: Spatial filtering of daily positions for estimating coseismic and postseismic displacements induced by the 1992 Landers earthquake. *Journal of Geophysical Research*, *102*(B8), 18,057–18,070. https://doi.org/10.1029/97JB01378